Terahertz cyclotron emission of two-dimensional Dirac fermions

Sebastian Gebert, Christophe Consejo, Sergey Krishtopenko, Sandra Ruffenach, Maria Szola, Jeremie Torres, Cedric Bray, Benoit Jouault, Milan Orlita, Xavier Baudry, et al.

Terahertz cyclotron emission of two-dimensional Dirac fermions

Sebastian Gebert
Montpellier University
Christophe Consejo
Universite de Montpellier
Sergey Krishtopenko
CNRS
Sandra Ruffenach
CNRS
Maria Szola
Montpellier University
Jeremie Torres
University of Montpellier https://orcid.org/0000-0001-5874-0990
Cedric Bray
CNRS
Benoit Jouault
CNRS
Milan Orlita
French National High Magnetic Field Laboratory https://orcid.org/0000-0002-9633-507X
Xavier Baudry
CEA
Philippe Ballet
CEA
Sergey Morozov
Institute for Physics of Microstructures, Russian Academy of Sciences
Vladimir Gavrilenko
IPM RAS
Nikolai Mikhailov
Institute of Semiconductor Physics
Sergei Dvoretskii
Institute of Semiconductor Physics
Frederic Teppe (Frederic.Teppe@umontpellier.fr)
CNRS-UM Laboratoire Charles Coulomb (L2C)

Article

Keywords:

Posted Date: June 1st, 2022

DOI: https://doi.org/10.21203/rs.3.rs-1630601/v1

Terahertz cyclotron emission of two-dimensional Dirac fermions

S. Gebert[1,2‡], C. Consejo[1‡], S.S. Krishtopenko[1], S. Ruffenach[1], M. Szola[1], J. Torres[2], C. Bray[1], B. Jouault[1], M. Orlita[3,4], X. Baudry[5], P. Ballet[5], S.V. Morozov[6,7], V.I. Gavrilenko[6,7], N.N. Mikhailov[8,9], S.A. Dvoretskii[8,10], F. Teppe[1*]

[1] Laboratoire Charles Coulomb (L2C), UMR 5221 CNRS-Université de Montpellier, F-34095 Montpellier, France

[2] Institut d'Electronique et des Systèmes (IES), UMR 5214 CNRS, Université de Montpellier, Montpellier 34095, France

[3] Laboratoire National des Champs Magnétiques Intenses, CNRS-UGA-UPS-INSA-EMFL, Grenoble, France

[4] Institute of Physics, Charles University, CZ-12116 Prague, Czech Republic

[5] CEA, LETI, MINATEC Campus, DOPT, 17 rue des martyrs 38054 Grenoble Cedex 9, France

[6] Institute for Physics of Microstructures of Russian Academy of Sciences, 603950, Nizhny Novgorod, Russia

[7] Lobachevsky State University of Nizhny Novgorod, 603950, Nizhny Novgorod, Russia

[8] A.V. Rzhanov Institute of Semiconductor Physics, Siberian Branch of Russian Academy of Sciences, 630090 Novosibirsk, Russia

[9] Novosibirsk State University, 630090, Novosibirsk, Russia

[10] Tomsk State University, Tomsk, Russia

‡ These authors have contributed equally to this work and share first authorship

* Corresponding author

Since the emergence of graphene, we have seen several proposals for the realization of Landau lasers tunable over the terahertz frequency range. The hope was that the non-equidistance of the Landau levels from Dirac fermions would suppress the harmful non-radiative Auger recombination. Unfortunately, even with this non-equidistance an unfavorable non-radiative process persists in Landau-quantized graphene, and so far no cyclotron emission from Dirac fermions has been reported. One way to eliminate this last non-radiative process is to sufficiently modify the dispersion of the Landau levels by opening a small gap in the linear band structure. A proven example of such gapped graphene-like materials are HgTe quantum wells close to the topological phase transition. In this work, we experimentally demonstrate Landau emission from Dirac fermions in such HgTe quantum wells, where the emission is tunable by both the magnetic field and the carrier concentration. Consequently, these results represent an advance in the realization of terahertz Landau lasers tunable by magnetic field and gate-voltage.

Introduction

The Cyclotron or Landau level emission occurs when non-equilibrium electrons, which are subject to an external magnetic field, recombine radiatively between two magnetic quantum levels, so-called Landau levels (LL). Considering a parabolic energy-momentum dispersion and the accumulation of all electrons in a single LL, n, the emission rate ($n \rightarrow n-1$) becomes proportional to n, while the absorption rate ($n \rightarrow n+1$) is proportional to $n+1$. Thus, in systems with parabolic dispersion, absorption always outweighs amplification. When, on the other hand, these electrons have relativistic energies, i.e. in systems with non-parabolic energy-momentum dispersion, the LLs become non-equidistant in energy, which makes it possible to overcome absorption losses. Structures with such non-parabolic energy-momentum dispersion are therefore a crucial factor for the development of cyclotron resonance sources. As a matter of fact, this emission process has for decades been the subject of a comprehensive study in the fields of plasma physics [1], vacuum electronics, and relativistic electronics

for the development of electron cyclotron masers [2,3] and free-electron lasers [4]. In parallel, and despite the fact that transitions between LLs are strongly affected by non-radiative processes [5], particular attention has been paid to semiconductors, in which the effective mass of charge carriers is small compared to the one of the free electrons, and thus, the splitting of LLs is much greater than in vacuum. Early theoretical studies in this field [6] showed that the nonlinear dynamics of charge carriers in the cyclotron resonance (CR) regime are the key ingredient for the generation and the amplification of electromagnetic radiation in semiconductors. In particular, Lax [7] was the first to demonstrate that the necessary conditions for cyclotron emission can be fulfilled in semiconductors having non-parabolic band dispersion. Indeed, as for electrons in vacuum, the resulting non-equidistance of LLs was supposed to decrease the probability of non-radiative Auger recombination (Fig. 1a). Later, Wolff [8] theoretically found that in semiconductors possessing strong interaction between charge carriers and optical phonons, the threshold nature of such interaction at low temperature ($k_B T \ll \hbar\omega_0$, where $\hbar\omega_0$ is the optical phonon energy) also results in LLs with unequal width (Fig. 1b). In fact, at low temperature, the spontaneous emission of optical phonons can only occur for charge carriers having energies $\mathcal{E} > \hbar\omega_0$. Therefore, the LL widths differ significantly for levels energies $\mathcal{E} > \hbar\omega_0$ and $\mathcal{E} < \hbar\omega_0$. Thus, the emission line is narrower than the absorption one, resulting in negative differential conductivity in a certain frequency range. (Fig 1b) [9,10]. Finally, semiconductors with a complex anisotropic band structure can also exhibit negative differential conductivity caused by a difference in polarization of the upward and downward optical transitions from a filled LL (Fig. 1c). This phenomenon occurs in negative effective mass amplifiers and generators (NEMAGs) [11] where the circular polarized light associated with negative cyclotron mass holes, interacts weakly with the positive cyclotron mass holes, which are associated with an opposite circular polarization. This discrimination between the different LLs can therefore lead to a negative differential conductivity and to a population inversion [12,13].

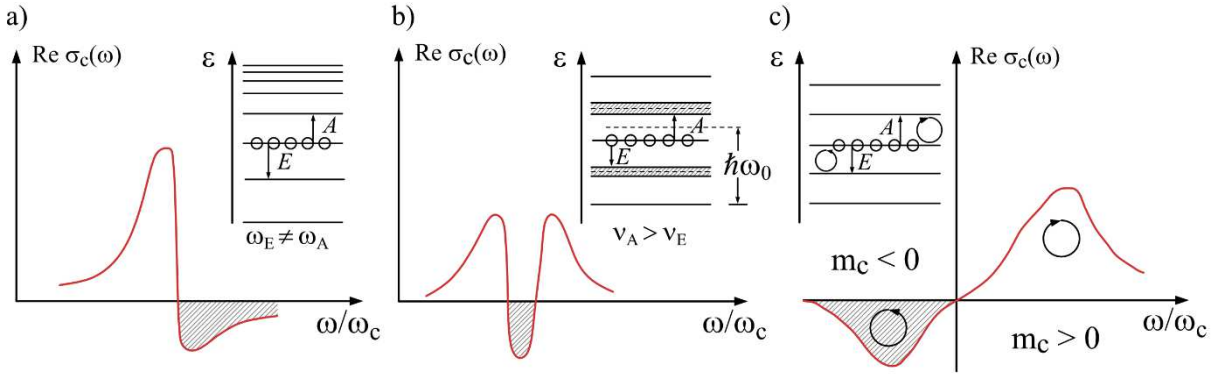

Fig. 1. Different mechanisms of negative differential conductivity in the cyclotron resonance regime in semiconductors arising in the case of a population inversion between LLs. The panels provide a qualitative representation of the CR differential conductivity $\mathrm{Re}\,\sigma_c(\omega)$, for the corresponding LL diagrams shown as insets. The areas corresponding to the negative values of $\mathrm{Re}\,\sigma_c(\omega)$ are shaded. a) Negative differential conductivity due to non-equidistant LLs. In vacuum electronics, this case is employed for gyrotrons [14,15], while for semiconductors it was first noticed by Lax [7]. b) Negative differential conductivity $\mathrm{Re}\,\sigma_c(\omega)$ due to the difference in width of the LLs. The CR amplification attributed to the differences in the LL widths was first observed by Hirshfield and Watchel [16] in gaseous plasma. c) Negative differential conductivity due to the difference in sign of the circular polarization of the transitions between LLs. The up and down transitions of the occupied LL indeed have different cyclotron mass signs and therefore resonate with different circular polarizations, resulting in stimulated emission in CR-based NEMAG.

Although the ideas for vacuum and semiconductor LL lasers arose simultaneously, their further development proceeded diversely. The active search for vacuum LL lasers led to the creation of gyrotrons [15,17,18], which still remain the most powerful sources of millimeter wave radiation. With regard to semiconductors, experimental research on solid-state LL lasers began in the 1970s, after realizing that scattering processes (especially inelastic scattering by optical phonons [19]) could induce a population inversion [20,21]. The Landau emission in the Far-Infrared and Terahertz (THz) range was

therefore intensively studied in different materials, as *n*-type InSb [22,23], GaAs [24,25], HgCdTe [26,27], Si-inversion layers [28]. Further development of the methods for numerical simulation of the scattering processes in electric and magnetic fields [29,30] revealed a number of new possibilities for inverted distribution of the charge carrier resulting in realization of light-hole [31] and light-heavy-hole LL laser [32,33], and CR-based NEMAG in bulk *p*-Ge [34,35]. Regarding the first two types of lasers [36], the population inversion is due to the accumulation of light holes in the vicinity of the optical phonon energy. The operation of these lasers requires the use of strong crossed electric and magnetic fields, which unfortunately brings the material closer to its electrical breakdown zone. CR-based NEMAG, on the other hand, does not require large electric and magnetic fields to trigger population inversion. However, this drastically limits the tunability range of its resonant frequency to 0.1–0.3 THz [35]. These *p*-Ge lasers remain to date the only semiconductor LL lasers ever implemented.

More recently, graphene and its linear band structure was also proposed as an interesting candidate towards a lossless Landau laser [37,38,39,40,41] operating with relatively low magnetic field on the principle of gyrotrons (see Fig. 1a). It was supposed to have the double benefit of reducing non-radiative Auger scattering, given the non-equidistance of its LLs, and of presenting an extreme tunability of the cyclotron radiation frequency in weak magnetic field, due to the low cyclotron mass of Dirac fermions[42]. This idea has been successfully verified recently in a gapless HgCdTe bulk crystal and interpreted as due to the strict non-equidistance of the LLs [43]. However, the population inversion of two-dimensional (2D) Dirac electrons in Landau quantized graphene had still not been observed until now. On the contrary, very fast dynamics was clearly observed during the resonant excitation of optical transitions between low-energy LLs in graphene under strong magnetic field [44]. Despite this LL non-equidistance, Auger scattering was identified as the predominant mechanism for carrier redistribution in Landau quantized graphene. Indeed, due to the square root dependence of the energy on the Landau level index, one can still find transitions that fulfill the energy conservation law, opening up the channel for Auger scattering [45,46]. This seemed to negate the chances of observing a cyclotron emission in graphene and any other 2D system with a conical band structure described by the Dirac Hamiltonian.

However, this situation is not futile for Dirac fermions arising in semiconductor quantum wells (QWs) (like HgTe/CdHgTe QWs [47,48] and InAs/Ga(In)Sb QWs [49,50]), whose specificities make it possible to overcome non-radiative Auger recombination. Here, the Dirac Hamiltonian describing the low-energy band structure of these QWs [51] has additional terms absent in graphene. These terms not only transform a trivial band insulator into a topological insulator (having an inverted bandgap), but also break equidistant LL subsets, which suppress Auger recombination for massless Dirac fermions. The latter makes semiconductor QWs particularly suitable candidates for gyrotron-like LL lasers with the highest tunability in the THz frequency range.

In this work, we report on the observation of electrically-driven cyclotron emission of 2D massive and massless Dirac fermions in HgTe/CdHgTe QWs due to the suppression of Auger scattering. Our experimental results show a continuous tunability of the emission frequency in magnetic field and in carrier concentration, over the range from 0.5 to 3 THz, thus covering the terahertz gap [52] over which a tunable laser source is still in great demand.

Results

Landau levels of Dirac fermions in HgTe QWs

The low-energy band structure in HgTe QWs in the vicinity of the Γ point of the Brillouin zone is analytically described within the Dirac-like Bernevig-Hughes-Zhang (BHZ) model [51]. This model takes into account the lowest electron-like level $E1$, formed by the Bloch functions at the Γ point of the Brillouin zone with the total angular momentum $m_J=\pm 1/2$, and the top hole-like level $H1$ formed by the Bloch functions of heavy-holes with $m_J=\pm 3/2$ [51]. In the basis $|E1,+\rangle$, $|H1,+\rangle$, $|E1,-\rangle$, $|H1,-\rangle$, the BHZ Hamiltonian is written as

$$H_{\mathrm{BHZ}}(\mathbf{k}) = \begin{pmatrix} H_+(\mathbf{k}) & 0 \\ 0 & H_-(\mathbf{k}) \end{pmatrix}, \quad (1)$$

where $\mathbf{k} = (k_x, k_y)$ is the momentum in the QW plane, and

$$H_+(\mathbf{k}) = (C - \mathbb{D}k^2)\sigma_0 + (M - \mathbb{B}k^2)\sigma_z + A(k_x\sigma_x + k_y\sigma_y). \quad (2)$$

Here, σ_0 is a 2×2 unit matrix, namely I_2, σ_α (with α=x, y or z) are the Pauli matrices, and C, M, A, $\mathbb{B}$, $\mathbb{D}$ are the structure parameters, which depend on the QW width, the barrier material, the QW growth direction and external conditions [53], respectively. The mass parameter M defines the band gap (which equals $2M$) at the Γ point ($\mathbf{k} = 0$) and the ordering of $E1$ and $H1$ subbands. For instance, the electron-like subband lies below the hole-like at $M < 0$. The blocks $H_+(\mathbf{k})$ and $H_-(\mathbf{k})$ in Eq. (1) describe the spin-up and spin-down electrons in the $E1$ and $H1$ subbands, respectively. Note that due to time reversal-symmetry $H_-(\mathbf{k}) = H_+^*(-\mathbf{k})$, where the star represents the complex conjugation. In Eq. (1), we have also neglected the small terms breaking inversion [54] and axial symmetries [55] around the growth direction, which results in the block-diagonal form of $H_{\mathrm{BHZ}}(\mathbf{k})$.

The structure parameters for the BHZ Hamiltonian (1) for a given HgTe QW, directly calculated on the basis of 8-band **k·p** Hamiltonian [53] by means of the procedure described elsewhere [56], are provided in Supplemental Materials.

The terms $\mathbb{D}k^2\sigma_0$ and $\mathbb{B}k^2\sigma_z$ in Eq. (2) quadratic in momentum are not present in the Dirac Hamiltonian familiar from relativistic quantum mechanics, but they play an important role in semiconductor QWs. In particular, the relative sign of $\mathbb{B}$ and M determines the Z_2 classification: the system is classified as a topologically trivial insulator if $M\mathbb{B} < 0$ and non-trivial insulator for $M\mathbb{B} > 0$ [51]. Since for HgTe QWs $\mathbb{B} < 0$, the inverted QW with $M < 0$ is thus a non-trivial topological insulator (for Fermi energies inside the gap), while the non-inverted QW with $M > 0$ is a trivial band insulator. The phase transition between these two types of insulators therefore occurs at $M = 0$, when the QW band structure mimics massless Dirac fermions.

The Hamiltonian (1) can be exactly diagonalized, and the two branches of doubly degenerated eigen-energies are:

$$E_s^{(\pm)}(\mathbf{k}) = C - \mathbb{D}k^2 + s\sqrt{(M - \mathbb{B}k^2)^2 + A^2k^2}, \quad (3)$$

where $s = +1$ (-1) stands for the conduction (valence) band, and the superscript ± of $E_s^{(\pm)}(\mathbf{k})$ stands for spin up (down) component, which are degenerated here.

To calculate LLs dispersion in the presence of an external magnetic field $\boldsymbol{B}$ oriented perpendicular to the QW plane, one should make the Peierls substitution of the momentum $\mathbf{k} \to -i\boldsymbol{\nabla} + e\mathbf{A}/c\hbar$ (where $\mathbf{A}$ is the vector potential so that $\boldsymbol{B} = \boldsymbol{\nabla} \times \mathbf{A}$) and add an additional Zeeman term H_Z to $H_{\mathrm{BHZ}}(\mathbf{k})$

$$H_Z = \frac{\mu_B B}{2}\begin{pmatrix} g_e & 0 & 0 & 0 \\ 0 & g_h & 0 & 0 \\ 0 & 0 & -g_e & 0 \\ 0 & 0 & 0 & -g_h \end{pmatrix}. \quad (4)$$

Here, μ_B is the Bohr magneton, and g_e and g_h are the g-factors describing the Zeeman splitting in $E1$ and $H1$ subbands, respectively. Solving the eigenvalue problem in the presence of magnetic field, the LL energies are found analytically [57]:

$$E_{n\geq 1}^{(\pm)} = C - \frac{2\mathbb{D}n \pm \mathbb{B}}{a_B^2} \pm \frac{g_e + g_h}{4}\mu_B B + s\sqrt{\left(M - \frac{2\mathbb{B}n \pm \mathbb{D}}{a_B^2} \pm \frac{g_e - g_h}{4}\mu_B B\right)^2 + \frac{2nA^2}{a_B^2}},$$
$$E_0^{(+)} = C + M - \frac{\mathbb{D} + \mathbb{B}}{a_B^2} + \frac{g_e}{2}\mu_B B,$$
$$E_0^{(-)} = C - M - \frac{\mathbb{D} - \mathbb{B}}{a_B^2} - \frac{g_h}{2}\mu_B B, \quad (5)$$

where a_B is the magnetic length ($a_B^2 = c\hbar/eB$). Typically in HgTe $g_e \gg g_h$ [58], so the latter can be neglected.

Figure 2 compares the LLs energies of Dirac fermions in graphene and HgTe QWs. As can be seen, in graphene (Fig. 2a), the perfect square-root dependence of the energy on the LLs indexes

counterintuitively opens a new channel for Auger scattering as its LLs spectrum ($E_n \propto \sqrt{n}$ for n = 0, 1, 2,…) includes subsets of equidistant levels [44,45]. In other words, the optical transition between LLs from n = 0 to n = 1 for instance, has the same energy as from n = 1 to n = 4, from n = 4 to n = 9, etc. Note that no equidistant LL subsets can be found for massive Dirac fermions, like relativistic electrons used in gyrotrons [17, 18]. The most essential difference between massless Dirac Fermions in semiconductor QWs and those in graphene is the absence of spin degeneracy of the LLs due to non-zero values of $\mathbb{B}$, $\mathbb{D}$, g_e and g_h. Importantly, due to these terms, it is then no longer possible to find series of equidistantly spaced LLs at a given magnetic field, as existing in graphene (Fig. 2b). Therefore, undesirable non-radiative Auger recombination may be suppressed for the Landau-quantized Dirac electrons in semiconductor QWs. Moreover, the band-gap *2M* for the Dirac fermions in semiconductor QWs can be tuned-at-will by adjusting the quantum confinement [47,48]. This band-gap opening further deviates the LL energies from the typical square root behavior known in graphene (see Fig.2c), which should decrease the non-radiative Auger recombination as well. Let us now show how these combined effects make possible to observe an efficient THz Landau emission in HgTe QWs.

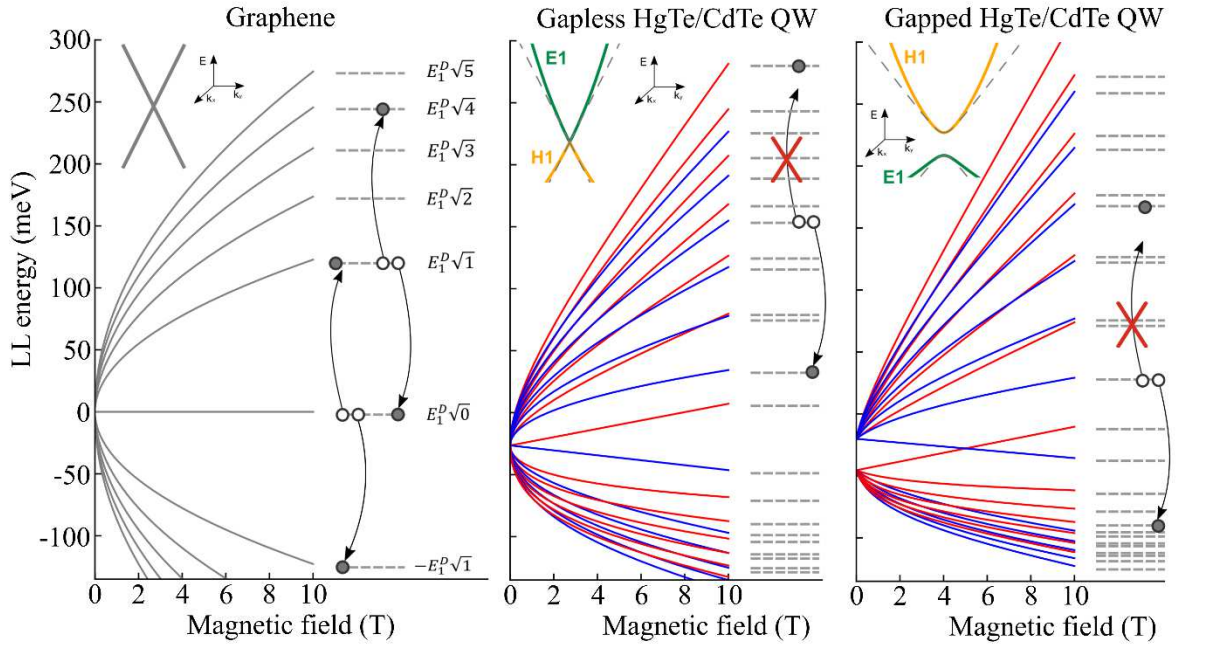

Fig. 2: **Landau levels of Dirac fermions in graphene and HgTe QWs**. (a) spin-degenerate Landau levels in graphene with the arrows indicating the LL subsets equally spaced in energy. The inset schematically illustrates the linear band dispersion. (b,c) Landau levels in gapless and inverted HgTe QWs. The red and blue curves correspond to the eigenvalues $E_n^{(+)}$ and $E_n^{(-)}$, respectively. The insets show the QW band structure. To stress the role of the quadratic terms, the dashed curves also represent the band structure at $\mathbb{B} = \mathbb{D} = 0$. The structure parameters used in the calculations are provided in Supplemental Materials.

THz cyclotron emission analysed by Landau spectroscopy

To observe the cyclotron emission of Landau-quantized Dirac electrons in HgTe QWs, we have employed a Landau spectroscopy technique. In cyclotron emission experiments, the radiation is generated by electrical excitations. The electrons in HgTe QWs are heated by electric field pulses, flattening the Fermi distribution and thus, populating upper empty Landau levels. These higher energy electrons then recombine by spontaneously emitting a photon at the energy difference between the Landau levels involved. Our Landau spectrometer (see Methods) can be used in two different modes. The first mode (Mode 1) consists in keeping the magnetic field applied to the detector constant, to fix the detection energy, while the magnetic field applied to the sample is scanned. The second mode (Mode 2) consists on the contrary in keeping the magnetic field on the sample constant by sweeping the one applied to the detector, to directly measure the emission spectrum. In order to favor the observation of

cyclotron radiation, we studied a series of HgTe QWs in the vicinity of its critical thickness corresponding to $M = 0$ (see Table 1 in Methods).

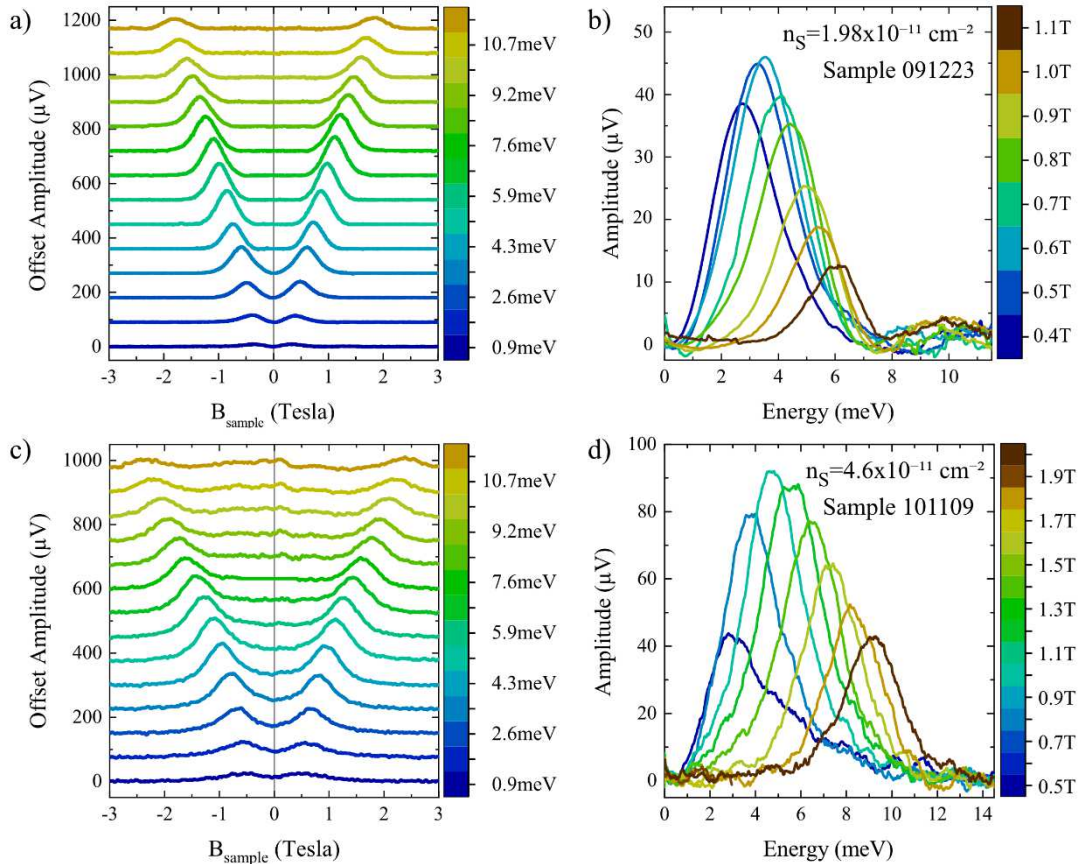

Fig. 3: **Cyclotron emission observed on 8 nm HgTe QWs, measured on two different samples at T = 4 K.** a) and c) The signal is recorded with an *n*-InSb detector by fixing the magnetic field applied to the detector, i.e. the detection energy (right panels), while sweeping the magnetic field applied on the sample. b) and d) The signal is measured while fixing the magnetic field applied to the sample (values of which are seen on the right side of these panels), as a function of the detector's energy, i.e. swiping the magnetic field on the detector side.

Figure 3 shows the cyclotron emission spectra of two 8 nm thick HgTe QWs of different electron concentrations. All spectra contain a clear emission line, symmetrical in positive and negative magnetic fields, and already visible at low energies (see Fig. 3 a) and c)). The line position clearly evolves linearly with the magnetic field, allowing determining the cyclotron mass. Note that the slope of the resonant energies as functions of magnetic field depends on the carrier concentration due to non-parabolic band structure of HgTe QWs (see Fig. 2(b,c)). Figures 3(b,d) provide the corresponding emission spectra measured at fixed magnetic field values for both samples. The emission peaks have a Gaussian-like shape, whose amplitudes increase first with the magnetic field and decrease after a certain energy value, which varies from one sample to another. Therefore, this non-monotonic evolution of the emission intensity cannot be attributed only to the reststrahlen band in the QWs (15–20 meV for $HgTe/Cd_xHg_{1-x}Te$), nor to the detector's limits. Indeed, *n*-InSb can be used as a narrow-band and tunable detector up to about 22 meV, where its efficiency is limited by the InSb reststrahlen band [59]. Moreover, depending on the carrier concentration, the edge of the reststrahlen band can be shifted towards energies slightly lower than 15 meV and it is therefore probable that the disappearance of the emission signal beyond 12 meV is due to the vicinity of the $HgTe/Cd_xHg_{1-x}Te$ reststrahlen band. However, the observed decrease in emission amplitude starts at much lower energies, on the order of 4 to 6 meV. This phenomenon therefore does not seem to be linked to the influence of the reststrahlen band. Another way to understand this behavior would be to consider that above the quantum limit, when the sample leaves

the incipient Landau quantization regime, the electron relaxation time decreases, as it was recently observed in graphene during the resonant excitation of optical transitions between low-energy LLs [44]. The reason may be due to the fact that despite of the non-equidistance of the Landau levels in HgTe QWs, it is still possible to find the states in the broadened LLs involved in optical transitions that fulfill the energy conservation and reactivate the Auger recombination. However, additional magneto-transport data (cf. the electron mobility μ in Table 1), obtained in the same experimental conditions, clearly show that this decrease in amplitude is not related to the quantum limit ($\mu B >> 1$). Therefore, we attribute this effect to the out-of-equilibrium carrier distribution in crossed electric and magnetic fields. Indeed, the carriers are in thermodynamic equilibrium during the magneto-transport measurements, while they are heated by short pulses of electrical excitation in the Landau emission experiments.

Cyclotron emission tunable in magnetic field and concentration

As discussed above, given the carrier mobility and the range of the applied external magnetic field, the samples are in the conditions of incipient Landau quantization. The low-index LLs are well separated, but given their non-equidistance, the distribution functions of the higher index states overlap to form a quasi-continuum. In this regime, the cyclotron frequency evolves linearly with the magnetic field and the system [60] can be treated in a semi-classical manner. The analytical form of $E_s^{(\pm)}(\mathbf{k})$ in Eq. (3) allows analytically calculating the cyclotron mass representing the resonant frequency of cyclotron emission. Applying a semi-classical quantization rule, the cyclotron mass m_c in the conduction band as a function of Fermi momentum $k_F = \sqrt{2\pi n_S}$ has the forms:

$$m_c = \frac{\hbar^2\sqrt{(M-\mathbb{B}k^2)^2+A^2k^2}}{s[A^2-2\mathbb{B}(M-\mathbb{B}k^2)]-2D\sqrt{(M-\mathbb{B}k^2)^2+A^2k^2}}. \quad (6)$$

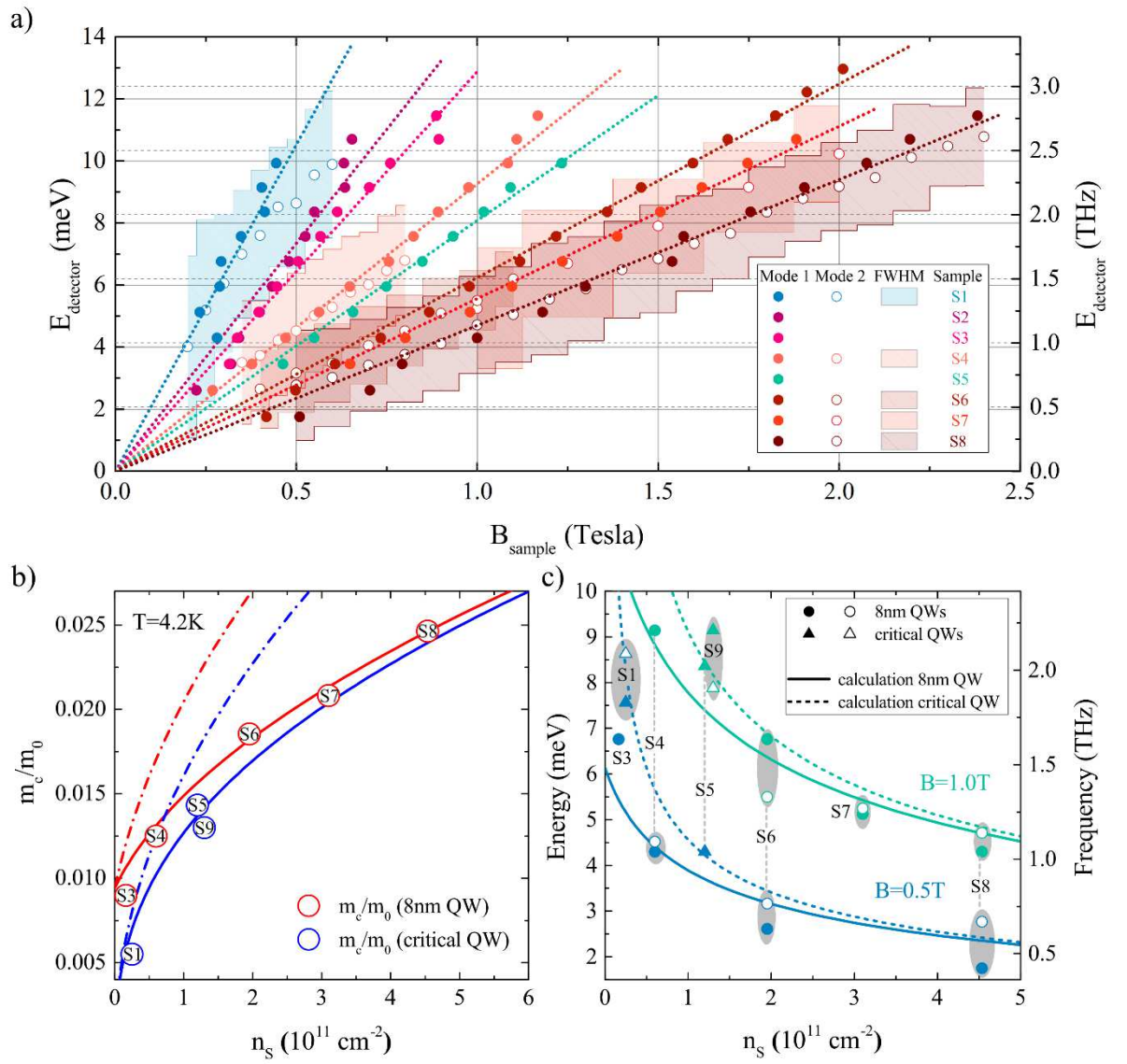

Fig. 4: **Analysis of the cyclotron emission energies.** a) Energy of the cyclotron emission peaks as a function of the magnetic field for various samples. The symbols correspond to the maximum intensity of the cyclotron resonance peak. The dotted lines are linear fits according to the classical cyclotron resonance condition from which the corresponding cyclotron mass values were extracted. b) The extracted cyclotron masses as a function of the carrier concentration of the samples in which the emission was measured. In this figure, the red and blue colors correspond to the QW thickness, 8 nm and critical, respectively. The solid curves represent the calculations based on Eq. (6). For comparison, we also provide the mass calculation within pure Dirac model involving only the linear terms i.e. at $\mathbb{B} = \mathbb{D} = 0$ (dashed lines). c) In order to highlight the tunability by concentration, we also represent experimental results by means of visualization of the energy and frequency emitted as a function of the density of carriers for two fixed magnetic fields, i.e. 0.5 Tesla and 1.0 Tesla. The shaded areas emphasize values extracted from the same sample with the two different operation modes, where full symbols represent again Mode 1 and open symbols Mode 2.

Figure 4 summarizes the position of the emission line at different magnetic fields and the corresponding cyclotron masses as functions of electron concentration extracted from magneto-transport data (see Supplemental Materials). It can be seen that even though the cyclotron mass was extracted from emission experiments with the out-of-equilibrium carrier distribution, its values are in good agreement with the theoretical mass at the Fermi level as a function of concentration calculated on the basis of

Eq. (6), as shown in Fig. 4(b). In order to emphasize the tunability of cyclotron radiation, Fig. 4(c) also shows the resonant energy for the two groups of QW widths at the two magnetic field values (0.5 T and 1 T). Here, we note a good agreement between the experimental values and the theoretical calculations in the energy range between 2 and 9 meV (0.5 to 2.2 THz). Additionally, the cyclotron mass extracted from emission results also agrees well with the results of magneto-absorption experiments performed on the same sample (see Supplemental Materials). Interestingly, the cyclotron resonance energy probed by magneto-absorption (cf. Supplementary Materials) is almost insensitive to temperature up to 100 K. The latter gives the hope to observe the Landau emission in HgTe QWs at significantly higher temperatures than the one observed in this work.

Discussion

Before discussing the conditions required for stimulated emission and gain, it is worth mentioning those for streaming effect and population inversion of the LLs. In the semi-classical regime, the homogeneous broadening of the cyclotron resonance, induced by elastic scattering on impurities and phonons, is directly related to the DC-conductivity at zero magnetic field[61]. The cyclotron resonance linewidth can therefore be compared with the reverse of the free carrier momentum relaxation time or total lifetime τ_t. The full-width at half-maximum of the emission lines in our experiments is on the order of 3-4 meV (corresponding to a frequency $f \approx 800$ GHz and a total life time $\tau_t \approx 0.2$ ps), which is about 10 times larger than the collision broadening values $\Delta\varepsilon = \hbar/\tau = \hbar e/\mu m_c$ extracted from mobility measurements (See Table 1 in Methods). It should also be noted that the linewidth of the emission line is twice that of the absorption (see Supplemental Materials). Indeed, spontaneous cyclotron emission involves hot electrons, which are distributed in a much broader energy range than the carriers probed by quasi-equilibrium magneto-absorption involving the electrons in the vicinity of Fermi energy. Therefore, the electric field yielding non-equilibrium electron distribution also influences the form of emission line in the systems with non-parabolic band structure – the cyclotron mass increases with the energy far from the band edge[62]. Additionally, the form of the emission line can be also affected by the inhomogeneous broadening due to electron-phonon scattering[63], as well the Stark broadening induced by ionized impurities[64]. The latter can be a dominant contribution into the emission linewidth as previously observed by Gornik et al. [65].

To evaluate the conditions required for streaming effect and possible population inversion of LLs, we compare the momentum relaxation time determined from the carrier mobility (see table 1 in Methods), with the time-of-flight T_{op} it takes for an electron to reach the longitudinal optical (LO) phonon energy[66] (18.3 meV for HgTe QWs [67]). With $T_{op} = \frac{V_{op} m_c}{eE}$ and $V_{op} = \sqrt{\frac{2\hbar\omega_{op}}{m_c}}$, we get $T_{op} \approx 6$ ps with typical electric field of about 100 V/cm used in our experiments. The momentum relaxation time determined by our transport measurements in on the order of 1–2 ps. In other words, the electrons are scattered before they reached the LO phonon energy. In order to reach E_{op} before scattering, the electron mobility should be of the order of $2{\cdot}10^5$ cm^2/V·s with an electric field from 300 to 600 V/cm. A population inversion would be possible only if the following condition were satisfied[68] $1 \leq \frac{V_{op}}{\left(\frac{E}{B}\right)} \leq 2$, which can be achieved, for instance, for an electric field of 2000 V/cm and magnetic field in the range from 0.2 to 0.4 T. These electric field values are achievable in sub-millimeter-sized grating gate devices fabricated from high-mobility HgTe QWs[69].

Let us now consider a lasing threshold in possible Landau laser based on Dirac fermions in HgTe QWs. In order to estimate the population inversion conditions, we assume inducing a gain comparable to that of THz p-Germanium lasers. The latter has typically a gain coefficient[70] $\gamma = N\left(\lambda^2/4\pi^2\,\tau_{sp}\Delta\nu\right)$ of the order of 0.05 cm^{-1} [71,72], where N corresponds to the population difference, λ is the wavelength of light in the medium and $\Delta\nu = 1/2\pi\,\tau_t$. In the case of relativistic electrons, the spontaneous cyclotron radiative lifetime can be appraised as follows[73]: $\tau_{sp}^{-1} = \alpha\left(\frac{v_F}{c}\right)^2 \omega_c$, where α is the fine structure constant, v_F and c are the Fermi and light velocities, respectively. In the THz frequency range, τ_{sp} is therefore on the order

of $1\ \mu s$, while $\tau_t \approx 0.2$ ps as was determined above. Therefore, if one considers for instance $\lambda = 300$ μm, it is necessary to carry out a population inversion of the order of $N \approx 1.7 \cdot 10^9$ cm^{-3}, which seems achievable in the pulsed excitation regime.

Conclusion

We have experimentally observed cyclotron emission of massive and massless Dirac fermions in HgTe QWs of different thicknesses. The emission is favored both by the gap opening and the specific band dispersion in HgTe QWs. The latter breaks the possibility to find series of equidistantly spaced Landau levels and thus suppresses non-radiative Auger recombination inherent in graphene. We have demonstrated a continuous tunability of the emission frequency in the range from 0.5 to 3 THz under low magnetic fields. These results lead us to consider HgTe QWs as promising materials for the development of a THz cyclotron laser largely tunable by a weak magnetic field or even by the gate voltage using a permanent magnet.

Methods

A part of the QWs were grown on GaAs (013) substrates with ZnTe and CdTe buffers (see Fig. M1 a) using molecular beam epitaxy (MBE) with *in situ* ellipsometric control[74] of the layer composition and thickness[75]. This growth method has been shown to provide high-quality structures, investigated in a large number of works [588,76]. The other part was grown on CdTe (001) substrate with again a CdTe buffer layer. The tensile strained HgTe well and HgCdTe barrier layers are grown at the same temperature (160°C) with a constant growth rate of 1 monolayer/s. Details on the growth and material characterization can be found in [77]and[78]. HgTe/CdTe structures grown using the same procedure are associated to high mobility electronic transport with clear Dirac characteristics [79] and have also been used to demonstrate record room-temperature spin to charge conversion [80](Fig. M1 a). The samples were cut into squares of approximately 5x5 mm^2 and gold wires were soldered to indium balls placed on the sample' surface, acting as ohmic contacts, spaced approximately 1 mm apart. The concentration and the mobility of the carriers were determined by magneto-transport measurements (detailed in the Supplementary Materials) whose results are grouped in Table 1. The experimental setup is a Landau spectrometer which consists of two independent 8 T and 14 T superconducting coils placed in the same cryostat (Fig. M1 b). The sample to be measured is positioned in the center of the first coil, while a magnetically tunable InSb photoconductive detector[81] is in the center of the second one. The InSb based cyclotron detector is a very sensitive detector with a spectral resolution on the order of 240 GHz (1 meV), over a spectral range from 0.8 THz up to 5 THz. The light emitted by the sample is guided toward the detector by a copper light pipe. The signal is detected as a voltage drop over the photoconductive detector, which is then amplified and measured via standard lock-in technique. The duty cycle (ratio of power-on to total time T_0) was set to a few percent (see Fig. M1 c) to prevent overheating of the sample, which would damage the sample and distort the signal. In our experiments, the electric pulses had peak-to-peak values V_A in the range of 10 to 100 V/cm and a duration t_{on} of a few milliseconds. The spectrometer can be used in two different modes of use. The first one consists in keeping constant the magnetic field applied to the InSb detector, so as to fix the detection energy, while the magnetic field applied to the sample is swept. The second mode consists on the contrary in fixing the magnetic field on the sample side and sweeping that applied to the detector, so as to directly measure the emission spectrum. Experimental details can be found in [82].

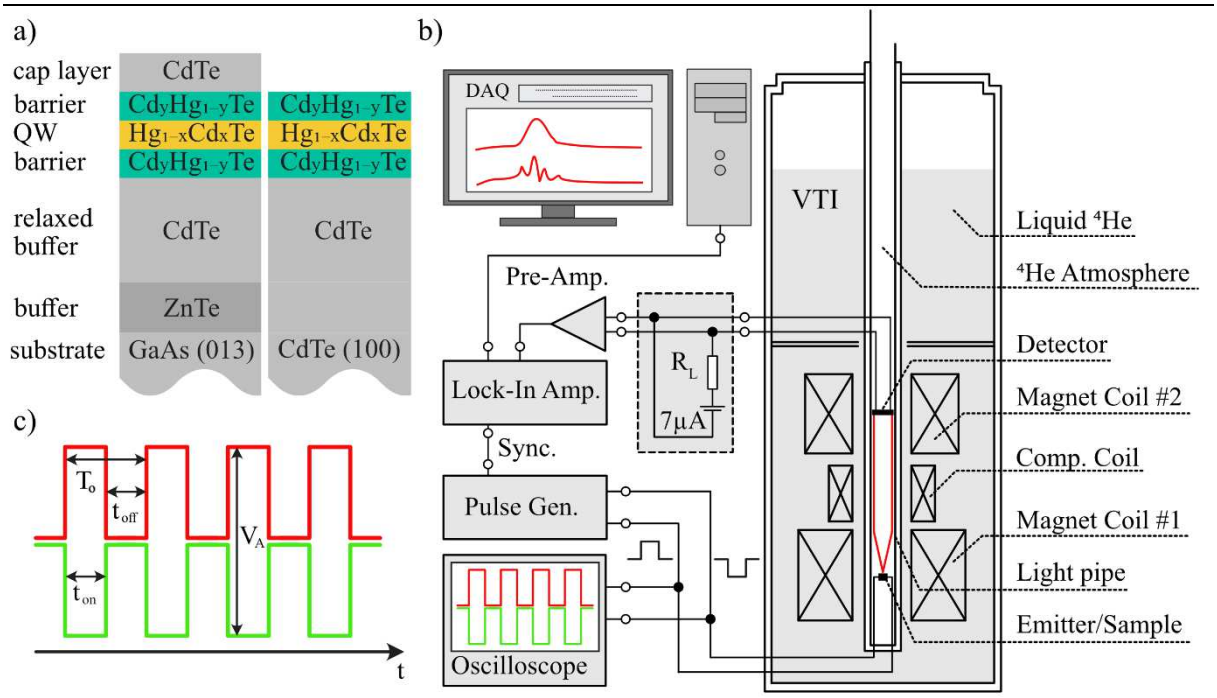

Fig. M1: Description of the Landau spectroscopy experimental setup. a) The samples are HgCdTe/CdHgTe QWs of different thicknesses and Cd compositions, on GaAs and CdTe substrates. b) The spectrometer is integrated in a cryostat and composed of two superconducting coils. One of them allows to apply a magnetic field to the measured sample while the other is applied to the cyclotron detector. A weaker third coil makes it possible to compensate for the action of the first on the second. The sample is excited by electrical pulses and the duty cycle of a few percent, detailed in c), is generally set to prevent overheating of the sample. The Landau emission signal is finally detected as a voltage drop across the InSb detector which is then amplified and measured via a standard lock-in technique.

Sample	Wafer	QW width (nm)	Gap width (meV)	Number of QWs	Carrier density $*10^{11}$ (cm^{-2})	Carrier mobility (cm^2/Vs)	Cyclotron mass m_c/m_e	FWHM (meV)	Collision broadening (meV)
S9	**130415**	6.3	~ 0	1	1.3	130 000	0.01249	-	0.71
S5	**101227**	6.5	~ 0	1	1.6	225 000	0.01433	-	0.36
S7	**091222-1**	8	28.1	1	3.1	190 000	0.02082	3.27	0.29
S6	**091223-1**	8	30.4	1	1.95	205 000	0.01855	2.51	0.30
S8	**101109**	8	-	1	4.58	154 000	0.02463	3.11	0.30
S2	**210702-5**	8.5	25-30	15	0.83	115 000	0.00788	-	1.27
S3	**170410**	8.0-8.2	-	50	0.23	80 000	0.00899	-	1.60
S1	**091225**	30	~ 0	1	0.5	105 000	0.0055	4.86	2
S4	**28104**	8	-	1	0.6	185 000	0.0125	3.58	0.5

Table 1: Parameters summary for the samples presented in this work. Carrier density and mobility are extracted from transport measurements (see supplementary information); other parameters are extracted from the emission data.

Additional information

The authors declare no competing financial interests. Correspondence and requests for materials should be addressed to F.T.

Acknowledgements

This work was supported by the Terahertz Occitanie Platform, by CNRS through IRP "TeraMIR", by the French Agence Nationale pour la Recherche (Colector and Stem2D projects), by the European Union through the Flag-Era JTC 2019 - DeMeGras project and the Marie-Curie grant agreement No 765426, from Horizon 2020 research and innovation program. The authors would like to thank Christian Lhenoret for technical support, Pr. Luca Varani for financial support, and Pr. Wojciech Knap for fruitful discussions and valuable support.

References

[1] R.Q. Twiss, Radiation Transfer and the Possibility of Negative Absorption in Radio Astronomy. Aust. J. Phys. 11, 564 (1958). https://doi.org/10.1071/PH580564
[2] J. L. Hirshfield and J. M. Wachtel, Electron cyclotron Maser, Phys. Rev. Lett. 12, 533 (1964)
[3] K. R. Chu, The electron cyclotron maser, Rev. Mod. Phys. 76, 489 (2004)
[4] P. G. O'Shea, H. P. Freund, Free-Electron Lasers : Status and Applications, Science 292, 5523, 1853 (2001)
[5] H. Dornhaus, K.-H. Muller, G. Nimtz, and M. Schifferdecker, Magnetic Quantum Oscillations in the Auger Transition Rate, Phys. Rev. Lett. 37, 11, 710 (1976)
[6] A.S. Tager, A.D. Gladun, Use of Cyclotron Resonance in Semiconductors for the Amplification and Generation of Microwaves. Sov. Phys. JETP 8, 560 (1959). http://www.jetp.ras.ru/cgi-bin/e/index/e/8/3/p560?a=list
[7] B. Lax, Cyclotron resonance and impurity levels in semiconductors : Proceedings of the International Symposium on Quantum Electronics, edited by C. H. Townes (Columbia Univ. Press, New York, 1960), p. 428
[8] P. A. Wolff, Proposal for a cyclotron resonance maser in InSb. Physics Physique Fizika 1, 147 (1964). https://doi.org/10.1103/PhysicsPhysiqueFizika.1.147
[9] J. Schneider, "Negative absorption of electromagnetic waves by electrons". Zeitschrift fur Naturforschung 15a, no. 5/6, 484 (1960) – in German. https://zfn.mpdl.mpg.de/data/Reihe_A/15/ZNA-1960-15a-0484.pdf
[10] J. M. Wachtel and J. L. Hirshfield, Phys. Rev. Lett. 19, 293 (1967)
[11] H. Kromer, Phys. Rev. 109, 1856 (1958); Proc. IRE 47, 397 (1959); Prog. in Semicond., Vol. 4, London, 1960, p. 3
[12] N.G. Basov, O.N. Krokhin, and Yu. M. Popov, Sov. Phys. JETP 11,720 (1960); Sov. Phys. Usp. 3, 702 (1961)
[13] Yu. Kogan, Sov. Phys. JETP 11, 1333 (1960)
[14] J. Schneider, Stimulated Emission of Radiation by Relativistic Electrons in a Magnetic Field. Phys. Rev. Lett. 2, 504 (1959)
[15] A. V. Gaponov, Interaction of irrectilinear electron beams with electromagnetic waves in transmission lines, lzv. Vuzov Radiofizika, vol. 2, pp. 450-462 (1959); Izv. Vuzov Radiofizika, vol 2, pp. 836-837, (1959), and A.V. Gaponov, M.I. Petelin, & V.K. Yulpatov, The induced radiation of excited classical oscillators and its use in high-frequency electronics. Radiophys. Quantum Electron. 10, 794–813 (1967) https://doi.org/10.1007/BF01031607
[16] J. M. Wachtel and J. L. Hirshfield, Phys. Rev. Lett. 19, 293 (1967)
[17] V. A. Flyagin, A. V. Gaponov, M. I. Petelin, and V. K. Yulpatov, IEEE Trans. Microwave Theory Tech. 25, 514 (1977)
[18] A.V. Gaponov, V.A. Flyagin, A.L. Goldenberg, G.S. Nusinovich, Sh.E. Tsimring, V.G. Usov, and S.N. Vlasov, Int. J. Electron. 51, 277 (1981)
[19] I.I. Vosilyus and I.B. Levinson. Sov. Phys. JETP 25, 672 (1967). http://www.jetp.ras.ru/cgi-bin/dn/e_025_04_0672.pdf
[20] W. Fawcett and H.D. Rees, Electron population inversion in GaAs induced by high electric fields. Phys. Lett. A 28, 731 (1969). https://doi.org/10.1016/0375-9601(69)90588-X
[21] H. Maeda, and T. Kurosawa, J. Phys. Soc. Jpn. 33, 562 (1972). https://doi.org/10.1143/JPSJ.33.562
[22] E. Gornik, "Recombination radiation from impact-ionized shallow donors in n-type InSb, " Phys. Rev. Lett., vol. 29, 595–597, (1972)
[23] K. L. I. Kobayashi, K. F. Komatsubara, and E. Otsuka, Tunable Far-Infrared Radiations from Hot Electrons in n-Type InSb, Phys. Rev. Lett. 30, 702 (1973); Erratum Phys. Rev. Lett. 31, 340 (1973)
[24] J. Waldman, T. S. Chang, H. R. Fetterman, G. E. Stillman, C. M. Wolfe, Recombination radiation from landau states in impactionized GaAs, Solid State Com. 15, 8, 1309 (1974). https://doi.org/10.1016/0038-1098(74)91369-6
[25] E. Gornik and R. Schawarz, Far infrared emission from 2D electrons at the GaAs/AlxGa1-xAs interface, Solid State Communications 38, 6, 541-545, (1981)
[26] E. Tyssen and G. Nimtz, Far infrared recombination radiation from n-type Hg1-xCdxTe Applied Optics 16, 11, 2957 (1977)

[27] E. Gornik, Far infrared cyclotron emission in semiconductors. J. Mag. Mag. Mater. 11, 39 (1979). https://doi.org/10.1016/0304-8853(79)90229-4
[28] E. Gornik and D.C. Tsui, Cyclotron and subband emission from Si-inversion layers, Surface Science 73, 217 (1978)
[29] Ya.I. Al'ber, A.A. Andronov, V.A. Valov, V.A. Kozlov, A.M. Lerner, I.P. Ryazantseva, Inverted hot-electron states and negative conductivity in semiconductors. Sov. Phys. JETP 45, 539 (1977). http://www.jetp.ras.ru/cgi-bin/e/index/e/45/3/p539?a=list
[30] C. Jacoboni and L. Reggiani Rev. Mod. Phys. 55, 645 (1983).
[31] Yu. L. Ivanov and Yu. V. Vasiljev, Stimulated Landau level emission in p-Ge. Sov. Tech. Lett. 9, 264 (1983).
[32] A. A. Andronov, I. V. Zverev, V. A. Kozlov, Yu. N. Nozdrin, S. A. Palor, and V. N. Shastin, Stimulated emission in the long-wavelength IR region from hot holes in Ge in crossed electric and magnetic field. Sov. Phys.-JETP Lett. 25, 804 (1984).
[33] S. Komiyama, N. Iizuka, and Y. Akasaka, Evidence for induced far-infrared emission from p-Ge in crossed electric and magnetic fields. Appl. Phys. Lett. 47, 958 (1985).
[34] A.A. Andronov, E.P. Dodin, and Z.F. Krasilnik, "Population inversion and CR negative differential conductivity of heavy hole in Ge under streaming", Fiz. Tech. Polupr. 16, 212 (1982) – in Russian
[35] A. A. Andronov, A. M. Belyantsev, V. I. Gavrilenko, E. P. Dodin, E. F. Krasil'nik, V. V. Nikonorov, S. A. Pavlov, and M. M. Shvarts, "Germanium hot-hole cyclotron-resonance maser with negative effective hole masses", Sov. Phys. JETP 63, 211, 1986 [Zh. Eksp. Teor. Fiz. 90, 367, 1986]. http://www.jetp.ras.ru/cgi-bin/dn/e_063_01_0211.pdf
[36] Y. L. Ivanov, Opt. Quantum Electron. 23, S253 (1991); Yu. A. Mityagin, V. N. Murzin, and S. A. Stoklitsky, Opt. Quantum Electron. 23, S287 (1991); V. N. Shastin, Opt. Quantum Electron. 23, S111 (1991).
[37] T. Morimoto, Y. Hatsugai, and H. Aoki, "Cyclotron radiation and emission in graphene - a possibility of Landau level laser," Journal of Physics: Conference Series 150, 022059 (2009)
[38] F. Wendler and E. Malic, "Towards a tunable graphene based Landau level laser in the terahertz regime," Scientific Reports 5 (2015)
[39] Y. Wang, M. Tokman, and A. Belyanin, Continuous-wave lasing between Landau levels in graphene. Phys. Rev. A 91, 033821 (2015).
[40] S. Brem, F. Wendler, and E. Malic, Microscopic modeling of tunable graphene-based terahertz Landau-level lasers. Phys. Rev. B 96, 045427 (2017)
[41] S. Brem, F. Wendler, S. Winnerl, and E. Malic, Electrically pumped graphene-based Landau-level laser. Phys. Rev. Materials 2, 034002 (2018).
[42] Y. Wang, M. Tokman, and A. Belyanin, "Continuous wave lasing between Landau levels in graphene," Phys. Rev. A 91, 033821 (2015)
[43] D. B. But, M. Mittendorff, C. Consejo, F. Teppe, N. N. Mikhailov, S. A. Dvoretskii, C. Faugeras, S. Winnerl, M. Helm, W. Knap, M. Potemski & M. Orlita, Suppressed Auger scattering and tunable light emission of Landau-quantized massless Kane electrons, Nature Photonics 13, 783–787 (2019)
[44] M. Mittendorff, F. Wendler, E. Malic, A. Knorr, M. Orlita, M. Potemski, C. Berger, W. A. de Heer, H. Schneider, M. Helm and S. Winner, Carrier dynamics in Landau-quantized graphene featuring strong Auger scattering, Nature Phyics, 11 75-81 (2015), 10.1038/NPHYS3164
[45] F. Wendler, A. Knorr, and E. Malic, Ultrafast carrier dynamics in Landau-quantized graphene, Nanophotonics 4, 224–249 (2015) DOI 10.1515/nanoph-2015-0018
[46] J. C. König-Otto, et al. Four-wave mixing in Landau-quantized graphene. Nano Lett. 17, 2184–2188 (2017).
[47] B. Büttner, C. Liu, G. Tkachov, E. Novik, C. Brüne, H. Buhmann, E. Hankiewicz, P. Recher, B. Trauzettel, S. Zhang, and L. Molenkamp, Single valley Dirac fermions in zero-gap HgTe quantum wells. Nat. Phys. 7, 418 (2011)
[48] M. Marcinkiewicz, S. Ruffenach, S. S. Krishtopenko, A.M. Kadykov, C. Consejo, D.B. But, W. Desrat, W. Knap, J. Torres, A.V. Ikonnikov, K.E. Spirin, S.V. Morozov, V.I. Gavrilenko, N.N. Mikhailov, S.A. Dvoretskii, and F. Teppe, Temperature-driven single-valley Dirac fermions in HgTe quantum wells. Phys. Rev. B 96, 035405 (2017)
[49] S. S. Krishtopenko and F. Teppe, Quantum spin Hall insulator with a large bandgap, Dirac fermions, and bilayer graphene analog. Sci. Adv. 4, eaap7529 (2018)
[50] S.S. Krishtopenko, W. Desrat, K.E. Spirin, C. Consejo, S. Ruffenach, F. Gonzalez-Posada, B. Jouault, W. Knap, K.V. Maremyanin, V.I. Gavrilenko, G. Boissier, J. Torres, M. Zaknoune, E. Tournié, and F. Teppe, Massless Dirac fermions in III-V semiconductor quantum wells. Phys. Rev. B 99, 121405(R) (2019)
[51] B.A. Bernevig, T.L. Hughes, and S.-C. Zhang, Science 314, 1757 (2006).
[52] Carlo Sirtori, Bridge for the terahertz gap, Nature 417, 132–133 (2002)
[53] S. S. Krishtopenko, I. Yahniuk, D. B. But, V. I. Gavrilenko, W. Knap, and F. Teppe, Phys. Rev. B 94, 245402 (2016)

[54] M. Konig, H. Buhmann, L. W. Molenkamp, T. Hughes, C.-X. Liu, X.-L. Qi, and S.-C. Zhang, J. Phys. Soc. Jpn. **77**, 031007 (2008).
[55] D. G. Rothe, R. W. Reinthaler, C.-X. Liu, L. W. Molenkamp, S.-C. Zhang, and E. M. Hankiewicz, New J. Phys. **12**, 065012 (2010).
[56] S. S. Krishtopenko, W. Knap, and F. Teppe, Sci. Rep. **6**, 30755 (2016).
[57] M. König, S. Wiedmann, C. Brüne, A. Roth, H. Buhmann, L. W. Molenkamp, X.-L. Qi, and S.-C. Zhang, Science 318, 766 (2007).
[58] A.M. Kadykov, S.S. Krishtopenko, B. Jouault, W. Desrat, W. Knap, S. Ruffenach, C. Consejo, J. Torres, S.V. Morozov, N.N. Mikhailov, S.A. Dvoretskii, and F. Teppe, Phys. Rev. Lett. **120**, 086401 (2018).
[59] L.H. Dmowski, M. Cheremisin, C. Skierbiszewski, W. Knap, Far-infrared narrow-band photodetector based on magnetically tunable cyclotron resonance-assisted transitions in pure n-type InSb, Acta Physica Polonica A, 4, 92, (1997)
[60] A. M. Witowski, M. Orlita, R. Stępniewski, A. Wysmołek, J. M. Baranowski, W. Strupiński, C. Faugeras, G. Martinez, and M. Potemski, Quasiclassical cyclotron resonance of Dirac fermions in highly doped graphene, Phys. Rev. B 82, 165305 (2010)
[61] D. J. Hilton, T. Arikawa, and J. Kono, Cyclotron resonance, Characterization of Materials, edited by Elton N. Kaufmann, (2012)
[62] E. Gornik, Landau emission in semiconductors. In: W. Zawadzki (eds) Narrow Gap Semiconductors Physics and Applications. Lecture Notes in Physics, vol 133. Springer, Berlin, Heidelberg (1980)
[63] C. Chaubet, A. Raymond, and D. Dur, Heating of two-dimensional electrons by a high electric field in a quantizing magnetic field: Consequences in Landau emission and in the quantum Hall effect, Phys. Rev. B 52, 11178 (1995)
[64] J. C. Hensel and Martin Peter, Stark effect for cyclotron resonance in degenerate bands, Phys. Rev. 114, 411 (1959)
[65] E. Gornik, R. Schawarz, G. Lindeman and D.C. Tsui, Emission spectroscopy on two-dimensional systems, Surface Science, 98, 493, (1980)
[66] S. Komiyama, Streaming motion and population inversion of hot carriers in crossed electric and magnetic fields, Advances in Physics, 31, 3, 255-297 (1982)
[67] D. Ushakov, A. Afonenko, R. Khabibullin, D. Ponomarev, V. Aleshkin, S. Morozov, and A. Dubinov, HgCdTe-based quantum cascade lasers operating in the GaAs phonon Reststrahlen band predicted by the balance equation method, Optics Express 28, 17, 25371-25382 (2020)
[68] S. Komiyama, T. Masumi, K. Kajita, Definite evidence for population inversion of hot electrons in silver halides, Phys. Rev. Lett. 42, 9 (1979)
[69] G. Tkachov, C. Thienel, V. Pinneker, B. Büttner, C. Brüne, H. Buhmann, L. W. Molenkamp, and E. M. Hankiewicz, Backscattering of Dirac Fermions in HgTe Quantum Wells with a Finite Gap, Phys. Rev. Lett. 106, 076802 (2011)
[70] B. E. A. Saleh and M. C. Teich, Fundamentals of Photonics 3rd edition (Wiley, 2019)
[71] K. Unterrainer, C. Kremser, E. Gornik, C. R. Pidgeon, Yu. L. Ivanov, and E. E. Haller, Tunable cyclotron-resonance laser in germanium, Phys. Rev. Lett. 64, 2277 (1990)
[72] H-W. Hubers, S. G. Pavlov and V. N. Shastin, Terahertz lasers based on germanium and silicon, Semicond. Sci. Technol. 20 S211–S221 (2005)
[73] T. Morimoto, Y. Hatsugai, and H. Aoki, Cyclotron radiation and emission in graphene. Phys. Rev. B 78, 073406 (2008)
[74] N. N. Mikhailov et al., Growth of $Hg_{1-x}Cd_xTe$ nanostructures by molecular beam epitaxy with ellipsometric control. International Journal of Nanotechnology 3, 120, doi:10.1504/ijnt.2006.008725 (2006); S.A. Dvoretsky et al., Growth of HgTe Quantum Wells for IR to THz Detectors. J. Electron. Mater., 39, 918 (2010). https://doi.org/10.1007/s11664-010-1191-7
[75] V. A. Shvets, N. N. Mikhailov, D. G. Ikusov, I. N. Uzhakov, & S. A. Dvoretskii, Determining the Compositional Profile of HgTe/CdxHg1–xTe Quantum Wells by Single-Wavelength Ellipsometry. Optics and Spectroscopy 127, 340-346, doi:10.1134/s0030400x19080253 (2019)
[76] S. Ruffenach et al., HgCdTe-based heterostructures for terahertz photonics. APL Materials 5, 035503, doi:10.1063/1.4977781 (2017)[77] P. Ballet, C. Thomas, X. Baudry, C. Bouvier, O. Crauste, T. Meunier, G. Badano, M. Veillerot, J.P. Barnes, P.-H. Jouneau and L.P. Lévy, J. Electron. Mater. 43, 2955 (2014)
[78] B. Haas, C. Thomas, P.-H. Jouneau, N. Bernier, T. Meunier, P. Ballet and J.L. Rouvière, Appl. Phys. Lett. 110, 263102 (2017)
[79] C. Thomas, O. Crauste, B. Haas, P.-H. Jouneau, C. Bäuerle, L.P. Lévy, E. Orignac, D. Carpentier, P. Ballet and T. Meunier, Phys. Rev. B 96, 245420 (2017)
[80] P. Noel, C. Thomas, Y. Fu, L. Vila, B. Haas, P.-H. Jouneau, S. Gambarelli, T. Meunier, P. Ballet and J.-P. Attané, Phys. Rev. Lett. 120, 167201 (2018)

[81] L. H. Dmowski, M. Cheremisin, C. Skierbiszewski, and W. Knap, “Far-infrared narrow-band photodetector based on magnetically tunable cyclotron resonance-assisted transitions in pure n-type InSb,” Acta Phys. Pol. A Gen. Phys., vol. 92, no. 4, pp. 733–736, 1997.
[82] W. Knap, D. Dur, and A. Raymond, A far-infrared spectrometer based on cyclotron resonance emission sources, Review of Scientific Instruments, vol. 63, p. 3293, (1992)

Supplementary Files

This is a list of supplementary files associated with this preprint. Click to download.

- SupplementaryInformationcorrectedfinal2.docx